

Finite-difference modeling of faults and fractures

Richard T. Coates* and Michael Schoenberg*

ABSTRACT

For the purposes of seismic propagation, a slip fault may be regarded as a surface across which the displacement caused by a seismic wave is discontinuous while the stress traction remains continuous. The simplest assumption is that this slip and the stress traction are linearly related. Such a linear slip interface condition is easily modeled when the fault is parallel to the finite-difference grid, but is more difficult to do for arbitrary nonplanar fault surfaces. To handle such situations we introduce equivalent medium theory to model material behavior in the cells of the finite-difference grid intersected by the fault. Virtually identical results were obtained from modeling the fault by (1) an explicit slip interface condition (fault parallel to the grid) and (2) using the equivalent medium theory when the finite-difference grid was rotated relative to the fault and receiver array. No additional computation time is needed except for the preprocessing required to find the relevant cells and their associated moduli. The formulation is sufficiently general to include faults in and between arbitrary anisotropic materials with slip properties that vary as a function of position.

INTRODUCTION

A fault is modeled as a fracture surface across which the traction is taken to be continuous (assuring finite particle acceleration), yet displacement is allowed to be discontinuous (slip occurs). The simplest model that accounts for the effect of such a surface on seismic waves allows the displacement discontinuity vector and the traction vector to be linearly related by a "fracture compliance matrix," \underline{Z} , i.e.,

$$\Delta \mathbf{u} = \underline{Z} \boldsymbol{\sigma} \cdot \mathbf{n}, \quad (1)$$

where $\Delta \mathbf{u}$ is the displacement discontinuity vector, and $\boldsymbol{\sigma} \cdot \mathbf{n}$ is the stress traction acting across the fracture (\mathbf{n} is the unit normal to the fracture). The compliance matrix \underline{Z} has dimensions *length/stress*. This is the linear slip deformation model, for example see Schoenberg (1980), Pyrak-Nolte et al. (1990a), although there has been earlier work considering similar formulations. This linear relationship is consistent with the usual seismic approximation of infinitesimal strain. In addition, there has been some experimental verification of the model in Pyrak-Nolte et al. (1990b) and Hsu and Schoenberg (1993).

This linearity condition is quite general, otherwise allowing for a completely anisotropic fracture response and also damping in the fracture response. The latter is achieved by allowing the fracture compliance matrix \underline{Z} to be a complex function of frequency with equation (1), then holding in the frequency domain and symbolizing a convolution in the time domain.

Essentially equation (1) is a boundary, or an interface, condition. In a finite difference algorithm it can be implemented by requiring a displacement jump across grid points on either side of the interface, proportional to the local (continuous) stress traction. Accurate implementation of such a displacement jump is relatively simple, even with \underline{Z} being a function of position on the fault plane, providing the interface lies along a given plane of the finite difference grid. Finite fractures can be considered simply by taking $\underline{Z} = 0$ at locations on the plane exterior to the fracture, the only remaining question being exactly how $\underline{Z} \rightarrow 0$ at the termination of the fracture, i.e., should \underline{Z} vanish abruptly or taper off (and if so how).

The question posed here is: "How may such a linear slip fracture be modeled when the fracture is at an angle to the finite difference grid?" To be included is the possibility that the fracture surface is not planar but a curved surface. The basic answer is that in each finite-difference cell intersected by the fracture, the elastic medium within the cell surrounding the fracture, together with the embedded segment of the fracture, are replaced by a suitable equivalent anisotropic medium. In two dimensions (2-D), cells are rectangles, and the fault is specified by a curve lying

Manuscript received by the Editor May 27, 1994; revised manuscript received November 7, 1994.

*Schlumberger Cambridge Research Ltd., High Cross, Madingley Road, Cambridge CB3 0EL, England.

© 1995 Society of Exploration Geophysicists. All rights reserved.

in the plane of wave propagation, the vertical x, z -plane, with waves generated by line sources parallel to the y -direction. In three dimensions (3-D), cells are rectangular parallelepipeds and the fault is a general smooth surface. The examples shown here consider only 2-D propagation with planar faults.

EQUIVALENT MEDIUM THEORY FOR ROCK NEAR A FRACTURE

Equivalent medium calculus is used to calculate the elastic parameters that are associated with a given cell through which the fault passes. From knowledge of the equivalent medium in each cell, it is a standard task to define the appropriate quantities to each point of the finite-difference grid. Muir et al. (1992) showed how the elastic parameters could be found for a cell enclosing an interface between two elastic media. The idea was to use the equivalent layered medium for the cell, where the layers were assumed parallel to the interface and the relative amount of each constituent was proportional to the amount of that constituent within the cell.

A fault or fracture, denoted by the dashed line in Figure 1, passing through a 2-D cell of area ΔA can be treated in a similar fashion. Consider the shaded region of area $h\Delta\ell$ surrounding the fault (here $\Delta\ell$ is the length of that segment of the fracture lying within the cell) and let the elastic moduli of that shaded region be proportional to h . In conventional condensed notation, the 6×6 elastic modulus matrix in the coordinate system of the fault, i.e., with x_3 normal to, and x_1 tangent to, the fault, may be written,

$$c_{ij} \equiv h\bar{c}_{ij}, \tag{2}$$

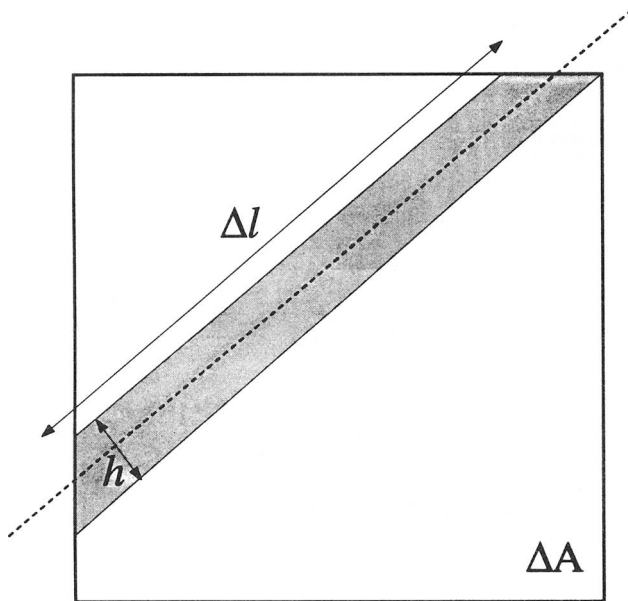


FIG. 1. A fault (dashed line) passing through a 2-D cell of area ΔA . $\Delta\ell$ is the length of the fault segment lying within the cell and h is the “thickness” of the fault (which in the limit goes to zero).

so the \bar{c}_{ij} have dimension *stress/length*. In the limit as $h \rightarrow 0$, the group element associated with the fracture in the fault coordinate system is, (Schoenberg and Muir, 1989),

$$\begin{aligned} g_f(1) &= 0, & g_f(2) &= 0, \\ g_f(3) &= \Delta\ell \begin{bmatrix} \bar{c}_{33} & \bar{c}_{34} & \bar{c}_{35} \\ \bar{c}_{34} & \bar{c}_{44} & \bar{c}_{45} \\ \bar{c}_{35} & \bar{c}_{45} & \bar{c}_{55} \end{bmatrix}^{-1} \equiv \Delta\ell \underline{Z}, \\ g_f(4) &= \mathbf{0}, & g_f(5) &= \mathbf{0}. \end{aligned} \tag{3}$$

Adding this to the group element of the nonfractured rock occupying the same cell of area ΔA , also in the fault coordinate system, and inverting to find the compliance matrix of the equivalent medium, yields the 6×6 compliance matrix, (Nichols et al., 1989, Hood, 1991),

$$\underline{s} = \underline{s}_b + \underline{s}_f = \underline{s}_b + \frac{\Delta\ell}{\Delta A} \underline{Z} \begin{bmatrix} 0 & 0 & 1 & 0 & 0 & 0 \\ 0 & 0 & 0 & 1 & 0 & 0 \\ 0 & 1 & 0 & 0 & 0 & 0 \\ 0 & 0 & 1 & 0 & 0 & 0 \\ 0 & 0 & 0 & 0 & 1 & 0 \\ 0 & 0 & 0 & 0 & 0 & 1 \end{bmatrix}, \tag{4}$$

where the subscript b denotes the background compliances, and the subscript f denotes the excess compliance of the cell as a result of the fault being modeled as a fracture surface. This carries over exactly to the 3-D case except ΔA is replaced by ΔV , the volume of the cell, and $\Delta\ell$ is replaced by Δa , the area of the fault or fracture lying within the 3-D cell volume. In either case, define L for each cell intersected by the fault so that,

$$\frac{1}{L} \equiv \frac{\Delta\ell}{\Delta A} \text{ for 2-D; } \quad \frac{1}{L} \equiv \frac{\Delta a}{\Delta V}, \text{ for 3-D.}$$

Inverting the compliance matrix, equation (4) gives the stiffness matrix for the cell in the fault coordinates system. In particular,

$$\underline{\epsilon} = \underline{s}^{-1} = [(\underline{I} + \underline{s}_f \underline{s}_b^{-1}) \underline{s}_b]^{-1} = \underline{\epsilon}_b (\underline{I} + \underline{s}_f \underline{\epsilon}_b)^{-1}. \tag{5}$$

A rotationally symmetric fault or fracture has a fracture compliance matrix of the form,

$$\underline{Z} = \begin{bmatrix} Z_N & 0 & 0 \\ 0 & Z_T & 0 \\ 0 & 0 & Z_T \end{bmatrix}, \tag{6}$$

where Z_T is the tangential compliance of the fracture and Z_N is the normal compliance of the fracture (Schoenberg, 1980). In this case, from equation (4),

$$\underline{s}_f = \frac{1}{L} \begin{bmatrix} 0 & 0 & 0 & 0 & 0 & 0 \\ 0 & 0 & 0 & 0 & 0 & 0 \\ 0 & 0 & Z_N & 0 & 0 & 0 \\ 0 & 0 & 0 & Z_T & 0 & 0 \\ 0 & 0 & 0 & 0 & Z_T & 0 \\ 0 & 0 & 0 & 0 & 0 & 0 \end{bmatrix}. \tag{7}$$

Thus, from equation (5),

$$\underline{\mathbb{I}} + \underline{\mathfrak{s}}_f \underline{\mathfrak{e}}_b = \underline{\mathbb{I}} + \frac{1}{L} \begin{bmatrix} 0 & 0 & 0 & 0 & 0 & 0 \\ 0 & 0 & 0 & 0 & 0 & 0 \\ Z_{NC13b} & Z_{NC23b} & Z_{NC33b} & Z_{NC34b} & Z_{NC35b} & Z_{NC36b} \\ Z_{TC14b} & Z_{TC24b} & Z_{TC34b} & Z_{TC44b} & Z_{TC45b} & Z_{TC46b} \\ Z_{TC15b} & Z_{TC25b} & Z_{TC35b} & Z_{TC45b} & Z_{TC55b} & Z_{TC56b} \\ 0 & 0 & 0 & 0 & 0 & 0 \end{bmatrix} \quad (8)$$

If the background medium is isotropic with Lamé parameters λ and μ , the medium equivalent to a rotationally symmetric fault embedded in a cell of the isotropic background medium is transversely isotropic with its symmetry axis perpendicular to the fracture. The matrix in equation (8) reduces to

$$\underline{\mathbb{I}} + \underline{\mathfrak{s}}_f \underline{\mathfrak{e}}_b = \begin{bmatrix} 1 & 0 & 0 & 0 & 0 & 0 \\ 0 & 1 & 0 & 0 & 0 & 0 \\ Z_N \lambda / L & Z_N \lambda / L & 1 + Z_N (\lambda + 2\mu) / L & 0 & 0 & 0 \\ 0 & 0 & 0 & 1 + Z_T \mu / L & 0 & 0 \\ 0 & 0 & 0 & 0 & 1 + Z_T \mu / L & 0 \\ 0 & 0 & 0 & 0 & 0 & 1 \end{bmatrix}, \quad (9)$$

and in this case the inversion is quite simple. The explicit form of the equivalent medium stiffness matrix in the coordinate system of the fault from equation (5) is,

$$\underline{\mathfrak{e}} = \begin{bmatrix} (\lambda + 2\mu)(1 - r^2 \delta_N) & \lambda(1 - r \delta_N) & \lambda(1 - \delta_N) & 0 & 0 & 0 \\ \lambda(1 - r \delta_N) & (\lambda + 2\mu)(1 - r^2 \delta_N) & \lambda(1 - \delta_N) & 0 & 0 & 0 \\ \lambda(1 - \delta_N) & \lambda(1 - \delta_N) & (\lambda + 2\mu)(1 - \delta_N) & 0 & 0 & 0 \\ 0 & 0 & 0 & \mu(1 - \delta_T) & 0 & 0 \\ 0 & 0 & 0 & 0 & \mu(1 - \delta_T) & 0 \\ 0 & 0 & 0 & 0 & 0 & \mu \end{bmatrix}, \quad (10)$$

$$r \equiv \frac{\lambda}{\lambda + 2\mu} = \frac{\nu}{1 - \nu},$$

$$\delta_T = \frac{Z_T \mu / L}{1 + Z_T \mu / L} = \frac{Z_T \mu}{L + Z_T \mu},$$

$$\delta_N = \frac{Z_N (\lambda + 2\mu) / L}{1 + Z_N (\lambda + 2\mu) / L} = \frac{Z_N (\lambda + 2\mu)}{L + Z_N (\lambda + 2\mu)},$$

where ν is the background Poisson's ratio. Thus even if Z_T and Z_N are assumed constant along the fault, the medium

parameters vary from cell to cell as a result of L varying from cell to cell.

The final step is to obtain the components of the stiffness matrix in the grid coordinate system. In 2-D, this entails a coordinate transformation about the y -axis; in 3-D the rotation to grid coordinates consists, in the most general case, of rotations about the three Euler angles.

INCLUSION OF FRACTURES IN THE FINITE DIFFERENCE SCHEMES

The examples shown in this paper are calculated using a standard staggered-grid, velocity-stress 2-D algorithm (Virieux, 1986) where the different components of the stress tensor are defined at different places. We shall be concerned with several overlapping arrays of such cells associated with the various components and distinguish between these arrays of cells only where necessary. Figure 2 shows the staggered grid and the locations at which the different components of the stress and velocity are defined. Similarly, the density and the various elements of the elastic tensor are

required at different locations. The density is needed where the velocities are defined, the elements c_{1i} and c_{3i} , $i = 1, \dots, 6$ are required where the diagonal stresses σ_{xx} , σ_{zz} are defined, and the components c_{5i} , $i = 1, \dots, 6$ are required where the off-diagonal stress σ_{xz} are defined.

Usually all medium parameters are specified initially at one point within the cell, for example at the diagonal stress locations. The parameters are then interpolated to where they are required using suitable interpolation functions. Muir et al. (1992) showed that it was preferable, particularly in the presence of strong variations (interfaces), to use effective media theory to correctly weight the effects of the different media within each cell according to their volume and orientation. This requires more detailed information concerning the location of the interface and a slightly more complicated calculation than simple averaging, but the extra cost of precomputing these medium parameters are negligible.

We follow Muir et al. (1992) but the situation is slightly more complicated because the different elements of the elastic stiffness matrix are required at different points on the staggered-grid as explained above. This minor complication

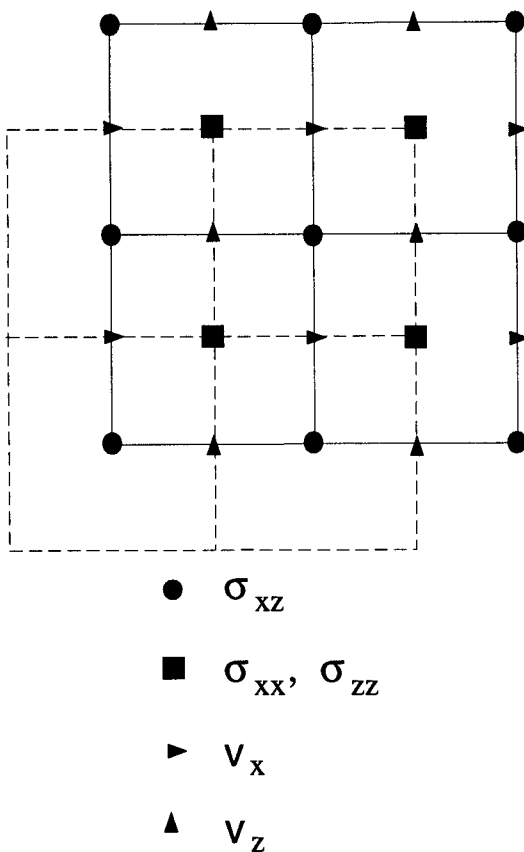


FIG. 2. The staggered grid used for the 2-D finite-difference scheme. The diagonal and off-diagonal components of the stress are defined at different points, as are the two components of the particle velocity. Different elements of the elastic modulus matrix are required at different points. For example c_{1i} and c_{3i} are required at the locations of the diagonal stresses and are effected by the medium and faults within the cells bounded by solid lines. The c_{5i} elastic moduli are required at the locations of the off-diagonal stresses and are effected by the medium and faults within the cells bounded by the dashed lines.

is included easily where necessary by staggering the cells used to calculate the different components of the effective media. Of course this complication is not present at all in formulations (e.g., pseudospectral) where all the variables are located at the same points.

The variables required for the effective medium calculation in each cell are the length of the fault (area of fault plane in 3-D) in each cell, its orientation, and the local value of the fracture compliance matrix Z . We choose to describe faults as a polynomial in the horizontal coordinate x . At each value of $x = i\Delta x$, $i = 0, \dots, i_{max}$, the polynomial is evaluated and a linear interpolation between adjacent values is carried out enabling the length of fault intersecting each cell and its orientation to be obtained using trivial algebra (Figure 3). The effective medium for each cell may then be calculated using these values and the theory outlined in the previous section.

In a general model some parts of the fault may lie between identical media, and the process outlined above will suffice. However, the fault will often separate different media because of a finite throw along the fault. In this case, an effective medium for the two media, in the absence of the fault, may be calculated using the effective medium calculus (Schoenberg and Muir, 1989) as in the case of a bonded interface (Muir et al., 1992), and this intermediate effective medium and the fault may be combined as described above.

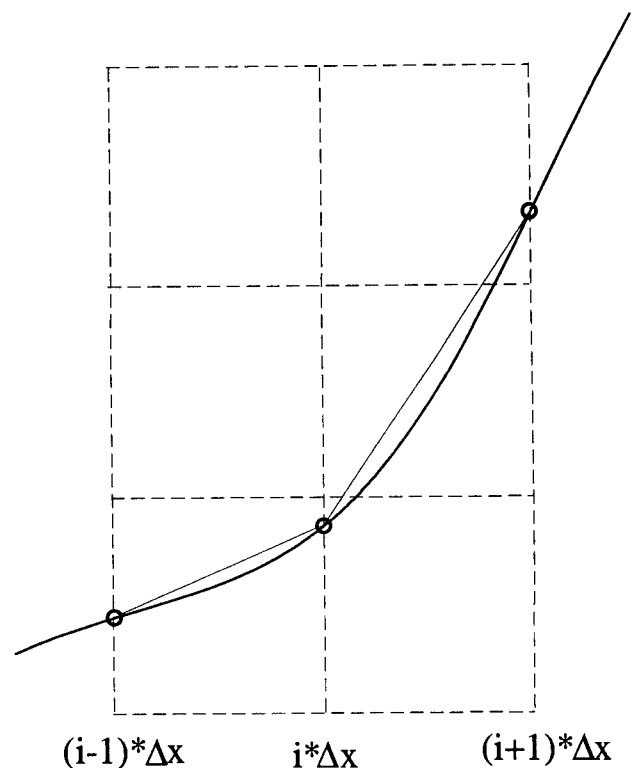


FIG. 3. The points at which a fault (heavy line) intersects vertical edges of each cell (circles) are evaluated from the polynomial specification of the fault. Linear interpolation (light line) is used to locate intersections of the fault with horizontal boundaries of each cell (if any) and to calculate the length and orientation of the fault lying in each cell.

There are two steps in validating this modeling method. The first step, which we will address here, compares results generated by the effective medium modeling with those produced by an explicit implementation of the boundary conditions, equation (1). The implementation of the explicit boundary conditions are outlined in Appendix B, and numerical comparisons are shown in the next section.

The second step in the validation process concerns the accuracy of the linear slip condition itself. This can be assessed only by comparison with field data and is not the subject of this paper. Similar work is needed to address the question of slip variation near the end of faults: does slip stop abruptly or taper off gently, or does the fault terminate in an extended zone of highly damaged material?

NUMERICAL EXAMPLES

In this section, we present modeling results designed to validate the effective medium model of the fault boundary conditions given in equation (1). To achieve this we show synthetics generated using the effective medium theory and using the explicit implementation of the boundary conditions outlined in Appendix B.

The case we examine is a horizontal fault in a transversely isotropic (TI) medium. The medium parameters are those of Greenhorn Shale (Jones and Wang, 1981), i.e., $c_{11} = 22.70$ GPa, $c_{33} = 34.30$ GPa, $c_{13} = 10.70$ GPa, and $c_{55} = 5.40$ GPa with the 1-direction taken horizontal (parallel to the fault) and the 3-direction vertical (normal to the fault). The density is $\rho = 2.37$ g/cm³. Note that in the strictly 2-D cases we shall examine and for polarizations in the plane of propagation, a TI medium is indistinguishable from a symmetry plane of an orthorhombic medium.

Figure 4 shows the experimental geometry. The receiver arrays at which vertical and horizontal particle velocity are recorded are arranged horizontally above and below the fault at a distance of 150 m from the fault. The maximum source-to-receiver vertical offset is 380 m. The fault itself is 760 m long with a boxcar compliance matrix falling abruptly to zero at each end. Within the boxcar, $Z_N = 0.1\Delta z/c_{11}$ and $Z_T = 0.2\Delta z/c_{55}$. This corresponds to an extra displacement

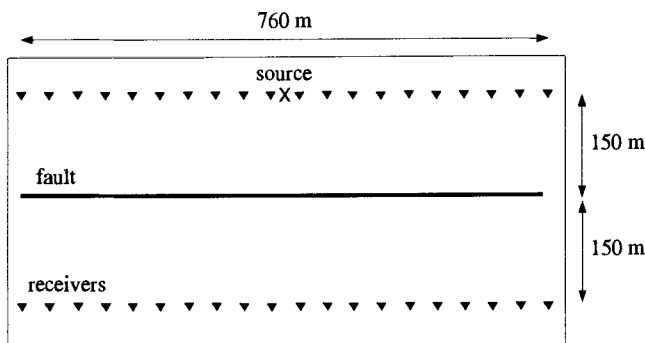


FIG. 4. The geometry used for the synthetic experiment. Vertical and horizontal particle velocities are recorded at two arrays 150 m above and below the fault. Each receiver array has an aperture of 760 m, equal to the length of the fault. The diagonal stress source is located at the center of the upper array.

across the grid containing the fault of approximately 10% for motion normal to the fault and 20% for transverse motion.

The source is located above the center of the fault and 150 m from it. The source wavelet is the second-derivative of a Blackman-Harris window with a duration of 10 ms and a dominant frequency of 100 Hz. The source is implemented as an excess isotropic stress by adding the same time series to each diagonal stress. We use a staggered-grid, velocity-stress, finite-difference scheme (Virieux, 1986) with fourth-order spatial differencing and second-order temporal differencing. The spatial-grid step is 1 m and the time step is 0.1 ms.

The direct signal, in the absence of the fault, is shown in Figure 5. The effect of the anisotropy is reflected in the presence of shear waves visible between 0.2 s and 0.27 s. In the examples presented below only the difference between the synthetics in the presence and absence of the fault will be shown.

First we examine the synthetics obtained when the fault lies parallel to the grid. Figure 6 shows synthetics generated using the explicit implementation (Appendix B) and the effective medium theory plotted on top of one another. The two methods produce results identical to within the thickness of a line. This result reflects the fact that the apparent stiffnesses implied by the explicit implementation (see equation (B-4)) are equivalent to those generated by the effective medium calculus. Note the waveform of the scattered signal is approximately one-time derivative of the incident signal. This is in agreement with the analytic reflection and transmission coefficients derived in Appendix A.

A more realistic test is shown in Figure 7. This relates to the case where the fault lies at an angle to the computational grid. To enable a comparison to be made with an explicit implementation of equation (1) we have rotated the fault about its central point through 45°. The source and receiver arrays have been rotated likewise to maintain the same relative location and orientation. Thus, the physical geometry of the experiment is unchanged, only the orientation of the computational grid has altered. Figure 7 is analogous to Figure 6. The synthetics generated using the explicit implementation, with the fault parallel to the grid, are overlain by the results calculated using the effective medium theory and the fault intersecting the grid at 45°. The fit between the two approaches is excellent once again, indicating that the effective medium is an adequate implementation of the fault boundary condition, equation (1), when the fault lies at an oblique angle to the grid.

As a final example, we show a simple faulted layer model with a reverse VSP geometry, Figure 8. Both formations are isotropic. The parameters of formation 1 are $\lambda + 2\mu = 22.70$ GPa, $\mu = 5.40$ GPa, and density $\rho_1 = 2.37$ g/cm³. Formation 2 differs only in that the density is $\rho_2 = 2.844$ g/cm³, i.e., increased by 20% over formation 1. The scattered field in the presence of the fault plane is shown in Figure 9 (the direct wave is not shown). This includes the effect of the step in formation 2 and the slip interfaces. Figure 10 shows the scattered field generated with the slip interface alone, i.e., the effects of the impedance contrasts have been calculated assuming a welded fault plane and subtracted from Figure 9. Figure 10 is magnified by a factor of 5 relative to Figure 9 to help locate the signal generated by the fault and also indi-

cates the small size of the reflection produced by the slip interface. Large scattered signals are generated by large values of Z_N and Z_T . This is discussed further in the next section.

DISCUSSION AND CONCLUSION

Several questions regarding the modeling of slip faults still need to be considered. One of the issues is whether a realistic slip fault will be visible in seismic data when the material parameters are the same on both sides of the fault.

The issue of possible reflection coefficient amplitudes will be discussed below. Another issue that is not so easy to clarify is whether a slip surface is a realistic model for a fault. Initial laboratory experiments of Pyrak-Nolte et al. (1990a) and Hsu and Schoenberg (1993) seem to indicate that the model has some validity when looking at individual fracture surfaces. In addition, Peterson et al. (1993) have shown results obtained from small-scale crosswell experiments that appear to agree with the model. So the question really is whether or not a fault is just a large fracture surface. Alternatively, the

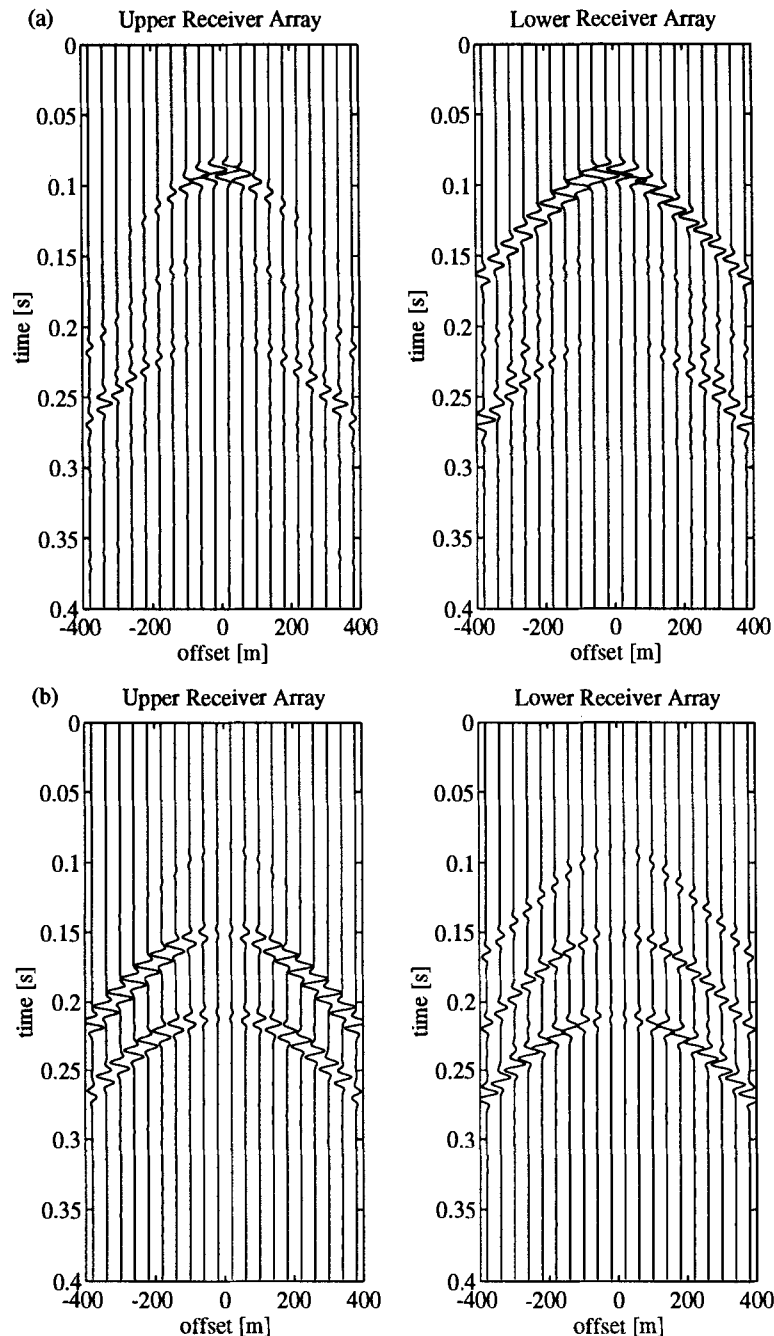


FIG. 5. (a) The vertical (normal to the fault) and (b) the horizontal (parallel to the fault) particle velocity in the absence of the fault. Note the anisotropic nature of the medium means the diagonal stress source generates shear as well as pressure waves. The triplication in the shear arrival can be seen at the extremes of the lower array.

question may be posed as to whether fracture compliances Z_N and/or Z_T are significantly larger than zero.

To get an idea of the order of magnitude and the phase change associated with reflection and transmission from a fault modeled by a slip interface, consider the simplest case of normal incidence of a plane wave in an isotropic medium on an up-down symmetric (relative to the fault plane) fault. In Appendix A, the reflection and transmission coefficient matrices are derived for general fault models embedded in an arbitrary anisotropic medium, subject only to the simplifying

assumption that the medium is up-down symmetric relative to the fault plane, and that the fault itself has up-down symmetry. This is ensured by letting the normal compliance of the fault be decoupled from the tangential compliances, i.e., there is no coupling between normal stress on the fault and tangential slip, or between shear stress on the fault and normal slip.

For P and SV propagation in a plane normal to the fault (the vertical here thought of as normal to the fault), as long as the fault itself does not couple P - and SV -waves into

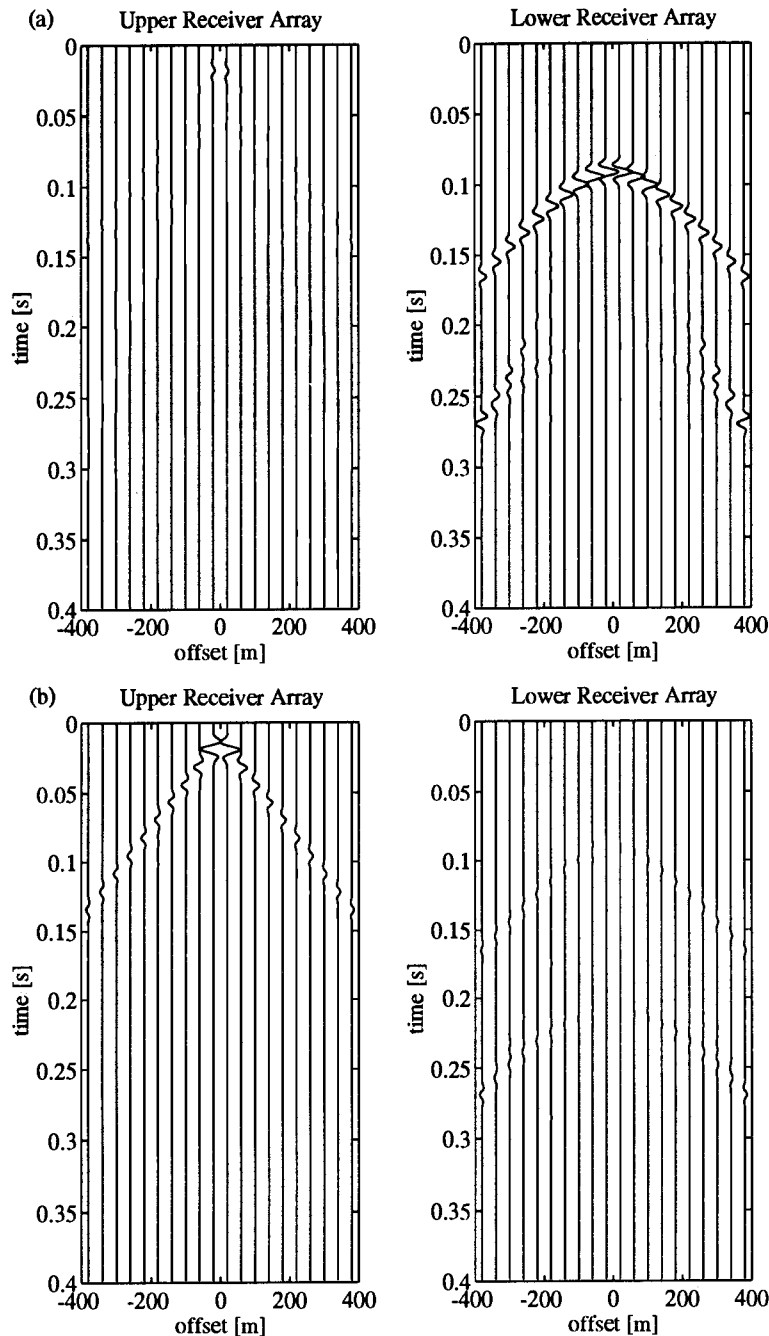


FIG. 6. The scattered wavefield generated by the fault, i.e., the difference between the wavefield in the presence and the absence of the fault. (a) The vertical (normal to the fault) and (b) the horizontal (parallel to the fault) particle velocities. The synthetics calculated using the explicit implementation and the effective medium theory are plotted on top of one another. The results are identical to within the thickness of a line.

SH-waves (which requires \underline{Z} to be diagonal) the 2-D formulation is adequate, and from equation (A-13) substituted into equation (A-12), subject to $p_1 = 0$ for normal incidence,

$$\underline{X}^{-1} \underline{Z}_T \underline{Y} = -Z_T \frac{\mu}{\beta} \begin{bmatrix} 0 & 0 \\ 0 & 1 \end{bmatrix}, \quad (11)$$

$$\underline{Y}^{-1} \underline{Z}_N \underline{X} = -Z_N \frac{\lambda + 2\mu}{\alpha} \begin{bmatrix} 1 & 0 \\ 0 & 0 \end{bmatrix}.$$

Remembering that the components of \underline{Z} have dimensions of *length/stress*, let,

$$Z_N \equiv \frac{\Delta}{\lambda + 2\mu} E_N, \quad Z_T \equiv \frac{\Delta}{\mu} E_T.$$

Then the substitution of equation (11), using these definitions, into equation (A-7) yields,

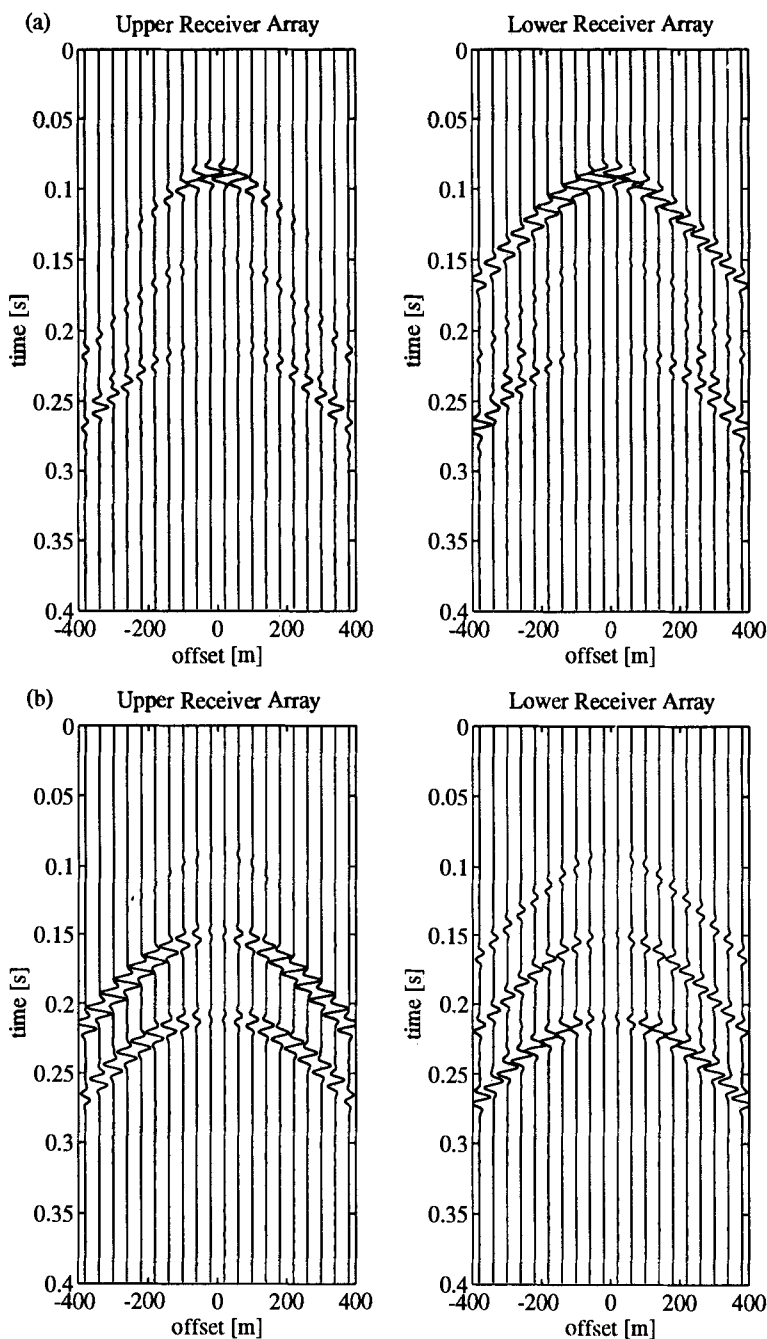


FIG. 7. The scattered wavefield generated by the fault as in Figure 6, except now the effective medium theory synthetics are generated with the grid lying at 45° to the fault. The source and receiver locations have been rotated to maintain the same experimental geometry. The effective medium results are plotted on top of the synthetics generated using the explicit implementation and as shown in figure 6.

$$\mathbf{T} = \begin{bmatrix} (1 - i\omega\Delta E_N/2\alpha)^{-1} & 0 \\ 0 & (1 - i\omega\Delta E_T/2\beta)^{-1} \end{bmatrix},$$

$$\mathbf{R} = \frac{i\omega\Delta}{2} \times \begin{bmatrix} E_N/\alpha(1 - i\omega\Delta E_N/2\alpha)^{-1} & 0 \\ 0 & -E_T/\beta(1 - i\omega\Delta E_T/2\beta)^{-1} \end{bmatrix}. \quad (12)$$

For normal incidence there can be no converted waves under these conditions. Then for a frequency of 100 Hz, with $\alpha = 3000$ m/s, $\beta = 1000$ m/s, and grid spacing $\Delta = 2.5$ m,

$$R_{PP} = \frac{i\pi E_N/12}{1 - i\pi E_N/12}, \quad R_{SS} = -\frac{i\pi E_T/4}{1 - i\pi E_T/4},$$

and for values $E_N = .1$ and $E_T = .2$, the reflection coefficient amplitudes are given approximately by

$$|R_{PP}| \sim .025, \quad |R_{SS}| \sim .15,$$

and these are clearly large enough to be observed. Further work will illuminate the amplitude versus tangential (to the fracture plane) slowness response of such a linear slip plane.

A method for modeling the effects of a slip fault on seismic wave propagation in finite-difference code has been presented. The actual finite-difference code has been verified by comparison with the case of an explicit slip plane along the grid coordinates. The application of such capability is twofold. One, it provides a way to model a fault (neglecting the question of how to treat the ends of the fault) over a wide range of numerical methods, not merely staggered-grid,

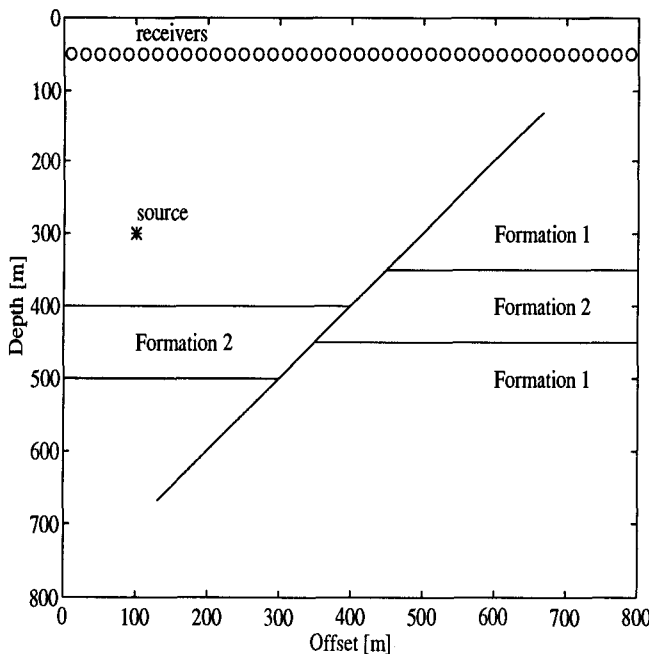


FIG. 8. A faulted layer model. Both formations are isotropic with $c_{ii} = 22.70$ GPa, $i = 1, 2, 3$ and $c_{ii} = 5.4$ GPa, $i = 4, 5, 6$. Formation 1 has a density $\rho_1 = 2.370$ g/cm³ and formation 2 has a density $\rho_2 = 2.844$ g/cm³. Synthetics are calculated both with and without the fault-plane slip condition.

finite-difference algorithms, and as such may provide clues as to what to look for in real data that would reflect the presence of, say, a “blind fault” in relatively homogeneous media. In particular, we have demonstrated the difference in the synthetic seismogram between modeling a normal fault without and with a slip condition across the fault. Second, the model provides a physically realistic way to construct a homogeneous velocity model with arbitrary dipping structure that can be used for testing imaging algorithms without raising the question of whether one has the correct velocity model. Previously, this was possible only under the unrealistic model of a constant velocity medium with significantly inhomogeneous density.

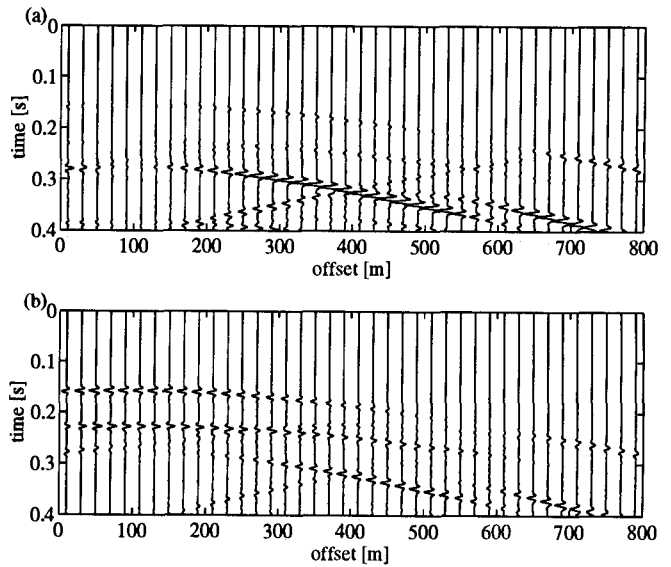


FIG. 9. The scattered field generated by the faulted layer model shown in Figure 8. (a) The horizontal particle velocity and (b) the vertical particle velocity. The X- and Y-components are plotted on the same scale.

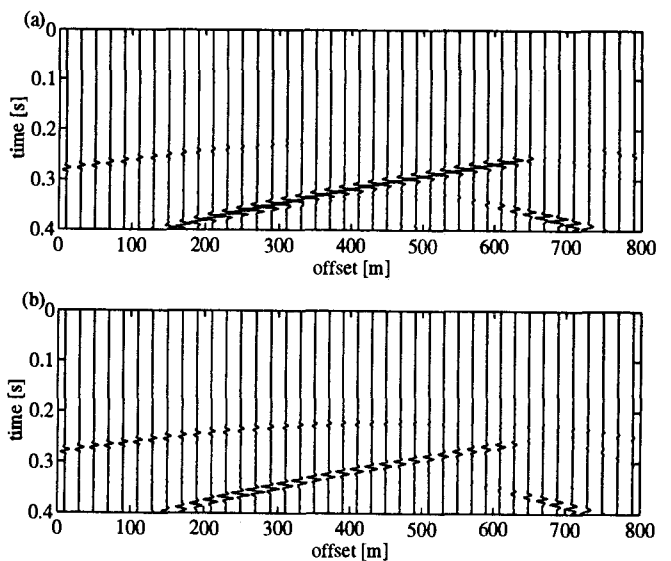


FIG. 10. The difference between the scattered field in the presence of the fault (slip) plane and in its absence. (a) The horizontal particle velocity and (b) the vertical particle velocity. The X- and Y-components are plotted on the same scale.

REFERENCES

- Hood, J., 1991, A simple method for decomposing fracture-induced anisotropy: *Geophysics*, **56**, 1275–1279.
- Hsu, C.-J., and Schoenberg, M., 1993, Elastic waves through a simulated fractured medium: *Geophysics*, **58**, 964–977.
- Jones, L. E. A., and Wang, H. F., 1981, Ultrasonic velocities in Cretaceous shales from the Williston Basin: *Geophysics*, **46**, 288–297.
- Muir, F., Dellinger, D., Etgen, J., and Nichols, D., 1992, Modeling elastic wavefields across irregular boundaries: *Geophysics*, **57**, 1189–1193.
- Nichols, D., Muir, F., and Schoenberg, M., 1989, Elastic properties of rocks with multiple fracture sets: 59th Ann. Internat. Mtg., Soc. Expl. Geophys., Expanded Abstracts, 471–474.
- Peterson, J. E., Hopkins, D., and Myer, L., 1993, Application of seismic displacement discontinuity theory to Hanford data: 63rd Ann. Internat. Mtg., Soc. Expl. Geophys., Expanded Abstracts, 1006–1009.
- Pyrak-Nolte, L. J., Myer, L. R., and Cook, N. G. W., 1990a, Transmission of seismic waves across single natural fractures: *J. Geophys. Res.*, **95**, B6, 8617–8638.
- 1990b, Anisotropy in seismic velocities and amplitudes from multiple parallel fractures: *J. Geophys. Res.*, **95**, B7, 11345–11358.
- Schoenberg, M., 1980, Elastic waves across a linear slip interface: *J. Acoust. Soc. Am.*, **68**, 1516–1521.
- Schoenberg, M., and Muir, F., 1989, A calculus for finely layered anisotropic media: *Geophysics*, **54**, 581–589.
- Schoenberg, M., and Protazio, J., 1992, ‘Zoeppritz’ rationalized and generalized to anisotropy: *J. Seismic Expl.*, **1**, 125–144.
- Virieux, J., 1986, *P-SV* wave propagation in heterogeneous media: Velocity-stress, finite-difference method: *Geophysics*, **51**, 889–901.

APPENDIX A

REFLECTION AND TRANSMISSION OF PLANE WAVES AT A LINEAR SLIP INTERFACE

Schoenberg and Protazio (1992), described a scheme for the calculation of plane-wave reflection and transmission coefficients at an interface between two anisotropic half-spaces. The only restriction on the anisotropy was that both media had to be at least monoclinic (for elasticity, this is equivalent to having a mirror plane of symmetry), each with its mirror plane of symmetry parallel to the interface. For a horizontal interface, we say that both media had to have up-down symmetry.

The special quality of that scheme is that the reflection and transmission coefficient matrices are expressible in terms of two “impedance matrix” functions of horizontal slowness \underline{X} and \underline{Y} for each of the media. These matrices, defined in Schoenberg and Protazio (1992), relate the physical variables to the amplitudes of the down-going plane waves in the medium; i.e., they are defined by

$$\begin{aligned} \mathbf{b}_X(x_3) &= \underline{X}\underline{\Lambda}(x_3)\mathbf{d}, \\ \mathbf{b}_Y(x_3) &= \underline{Y}\underline{\Lambda}(x_3)\mathbf{d}, \end{aligned} \quad (\text{A-1})$$

where \mathbf{d} is the vector of the particle velocity amplitudes of the possible downgoing ($+x_3$ propagating) waves, $\underline{\Lambda}(x_3)$ is a diagonal matrix whose elements are $\exp(i\omega x_3 p_{3o})$, with p_{3o} being the possible values of vertical slowness for the given value of horizontal slowness. The power of this approach comes from the fact that for monoclinic media, if \mathbf{u} is the vector of the amplitudes of the possible upgoing waves,

$$\begin{aligned} \mathbf{b}_X(x_3) &= \underline{X}\underline{\Lambda}(x_3)\mathbf{u}, \\ \mathbf{b}_Y(x_3) &= -\underline{Y}\underline{\Lambda}(x_3)\mathbf{u}. \end{aligned} \quad (\text{A-2})$$

For 2-D propagation of in-plane waves in the x_1, x_3 -plane,

$$\mathbf{b}_X \equiv \begin{bmatrix} v_1 \\ \sigma_3 \end{bmatrix}, \quad \mathbf{b}_Y \equiv \begin{bmatrix} \sigma_5 \\ v_3 \end{bmatrix},$$

\underline{X} and \underline{Y} are 2×2 matrix functions of horizontal slowness p_1 and material properties, in particular, elastic stiffnesses c_{11} , c_{33} , c_{55} , c_{13} and density ρ , while,

$$\underline{\Lambda}(x_3) = \begin{bmatrix} \exp i\omega p_{3p} x_3 & 0 \\ 0 & \exp i\omega p_{3s} x_3 \end{bmatrix}.$$

For 3-D propagation in general, horizontal slowness is a vector with components p_1, p_2 , so that \underline{X} and \underline{Y} are 3×3 matrix functions of p_1, p_2 , all 13 monoclinic elastic stiffnesses and density ρ , while,

$$\underline{\Lambda}(x_3) = \begin{bmatrix} \exp i\omega p_{3p} x_3 & 0 & 0 \\ 0 & \exp i\omega p_{3s} x_3 & 0 \\ 0 & 0 & \exp i\omega p_{3T} x_3 \end{bmatrix}.$$

The subscript T here denotes the third possible wave type.

The welded interface conditions at a planar boundary perpendicular to the 3-axis are that \mathbf{b}_X and \mathbf{b}_Y are continuous. Consider two media in welded contact: (1) an upper unprimed medium occupying $x_3 < 0$ in which there are downward incident waves with amplitude vector \mathbf{i} and upward reflected waves with amplitude vector $\mathbf{r} = \underline{\mathbf{R}}\mathbf{i}$, and (2) a lower primed medium occupying $x_3 > 0$ in which there are downward transmitted waves with amplitude $\mathbf{t} = \underline{\mathbf{T}}\mathbf{i}$. From equations (A-1) and (A-2), welded interface conditions at the horizontal boundary between the two media have the form,

$$\begin{aligned} \underline{X}(\mathbf{I} + \underline{\mathbf{R}}) &= \underline{X}'\underline{\mathbf{T}}, \\ \underline{Y}(\mathbf{I} - \underline{\mathbf{R}}) &= \underline{Y}'\underline{\mathbf{T}}. \end{aligned} \quad (\text{A-3})$$

The reflection and transmission coefficient matrices are square 2×2 matrices in 2-D, with subscripts P and S , with the first subscript denoting the reflected or transmitted wave type, and the second denoting the incident wave type (in keeping with the subscript convention for matrices). In 3-D, the reflection and transmission coefficient matrices are 3×3 with subscripts P, S , and T . Equations (A-3) can be solved easily by premultiplying the first equation by \underline{X}^{-1} , the second by \underline{Y}^{-1} , adding and solving for $\underline{\mathbf{T}}$, then subtracting and solving for $\underline{\mathbf{R}}$. This procedure yields,

$$\begin{aligned} \underline{\mathbf{T}} &= 2(\underline{X}^{-1}\underline{X}' + \underline{Y}^{-1}\underline{Y}')^{-1}, \\ \underline{\mathbf{R}} &= (\underline{X}^{-1}\underline{X}' - \underline{Y}^{-1}\underline{Y}')(\underline{X}^{-1}\underline{X}' + \underline{Y}^{-1}\underline{Y}')^{-1}, \end{aligned} \quad (\text{A-4})$$

which is a valid solution for all noncritical (in the incident medium, i.e., $|\underline{\mathbf{X}}| \neq 0, |\underline{\mathbf{Y}}| \neq 0$) horizontal slownesses.

The problem to be solved using this formalism is to find $\underline{\mathbf{T}}$ and $\underline{\mathbf{R}}$ when the two media on either side of the interface are the same but particle velocity at the interface is not continuous. Rather the boundary condition is that of a linear slip interface, but note that up-down symmetry when applied to a slip interface, reduces to there being no coupling between normal displacement discontinuity and tangential components of traction (the shear stresses, σ_5 and σ_4) and also between tangential displacement discontinuity and the normal traction component σ_3 . Thus, from the definition of \mathbf{b}_X and \mathbf{b}_Y in either two or three dimensions, the velocity jumps in components that are components of \mathbf{b}_X or depend on traction components that are components of \mathbf{b}_Y , and vice versa. This may be written in submatrix form as

$$\begin{bmatrix} \mathbf{b}_X \\ \mathbf{b}_Y \end{bmatrix}_{0-} = \begin{bmatrix} \underline{\mathbf{I}} & i\omega \underline{\mathbf{Z}}_T \\ i\omega \underline{\mathbf{Z}}_N & \underline{\mathbf{I}} \end{bmatrix} \begin{bmatrix} \mathbf{b}_X \\ \mathbf{b}_Y \end{bmatrix}_{0+}, \tag{A-5}$$

which yields, from equations (A-1) and (A-2), the analog of equation (A-3). For this case of a slip interface between identical half-spaces,

$$\begin{aligned} \underline{\mathbf{X}}(\underline{\mathbf{I}} + \underline{\mathbf{R}}) &= (\underline{\mathbf{X}} + i\omega \underline{\mathbf{Z}}_T \underline{\mathbf{Y}}) \underline{\mathbf{T}}, \\ \underline{\mathbf{Y}}(\underline{\mathbf{I}} - \underline{\mathbf{R}}) &= (\underline{\mathbf{Y}} + i\omega \underline{\mathbf{Z}}_N \underline{\mathbf{X}}) \underline{\mathbf{T}}. \end{aligned} \tag{A-6}$$

Solving these equations in exactly the same way equations (A-3) were solved yields

$$\begin{aligned} \underline{\mathbf{T}} &= \left[\underline{\mathbf{I}} + \frac{i\omega}{2} (\underline{\mathbf{X}}^{-1} \underline{\mathbf{Z}}_T \underline{\mathbf{Y}} + \underline{\mathbf{Y}}^{-1} \underline{\mathbf{Z}}_N \underline{\mathbf{X}}) \right]^{-1}, \\ \underline{\mathbf{R}} &= \frac{i\omega}{2} (\underline{\mathbf{X}}^{-1} \underline{\mathbf{Z}}_T \underline{\mathbf{Y}} - \underline{\mathbf{Y}}^{-1} \underline{\mathbf{Z}}_N \underline{\mathbf{X}}) \\ &\quad \times \left[\underline{\mathbf{I}} + \frac{i\omega}{2} (\underline{\mathbf{X}}^{-1} \underline{\mathbf{Z}}_T \underline{\mathbf{Y}} + \underline{\mathbf{Y}}^{-1} \underline{\mathbf{Z}}_N \underline{\mathbf{X}}) \right]^{-1}. \end{aligned} \tag{A-7}$$

To see this in detail in three dimensions, $\underline{\mathbf{Z}}_T$ and $\underline{\mathbf{Z}}_N$ are 3×3 matrices which depend on all the tangential slip compliances, $Z_{T_1} > 0, Z_{T_2} > 0, Z_{12}$, such that $Z_{T_1} Z_{T_2} - Z_{12}^2 > 0$ (from positive definiteness of the slip compliance matrix), and on the normal slip compliance, $Z_N > 0$, respectively. The linear slip conditions for the full monoclinic case are,

$$\begin{aligned} u_1|_{0+} &= u_1|_{0-} + Z_{T_1} \sigma_5 + Z_{12} \sigma_4, \\ u_2|_{0+} &= u_2|_{0-} + Z_{12} \sigma_5 + Z_{T_2} \sigma_4, \\ \sigma_3|_{0+} &= \sigma_3|_{0-}, \\ \sigma_5|_{0+} &= \sigma_5|_{0-}, \\ \sigma_4|_{0+} &= \sigma_4|_{0-}, \\ u_3|_{0+} &= u_3|_{0-} + Z_N \sigma_3, \end{aligned}$$

which after differentiating by time (so that $u_i \rightarrow v_i$ and $\partial \sigma_j / \partial t \rightarrow -i\omega \sigma_j$) may be rewritten,

$$\begin{aligned} v_1|_{0-} &= v_1|_{0+} + i\omega(Z_{T_1} \sigma_5 + Z_{12} \sigma_4), \\ v_2|_{0-} &= v_2|_{0+} + i\omega(Z_{12} \sigma_5 + Z_{T_2} \sigma_4), \\ \sigma_3|_{0-} &= \sigma_3|_{0+}, \\ \sigma_5|_{0-} &= \sigma_5|_{0+}, \\ \sigma_4|_{0-} &= \sigma_4|_{0+}, \\ v_3|_{0-} &= v_3|_{0+} + i\omega Z_N \sigma_3, \end{aligned} \tag{A-8}$$

i.e.,

$$\underline{\mathbf{Z}}_T = \begin{bmatrix} Z_{T_1} & Z_{12} & 0 \\ Z_{12} & Z_{T_2} & 0 \\ 0 & 0 & 0 \end{bmatrix}, \quad \underline{\mathbf{Z}}_N = \begin{bmatrix} 0 & 0 & 0 \\ 0 & 0 & 0 \\ 0 & 0 & Z_N \end{bmatrix}, \tag{A-9}$$

in equation (A-5). Note that, in general, one can rotate the coordinate system about the x_3 -axis until the crossterm Z_{12} vanishes, leaving $\underline{\mathbf{Z}}_T$ a diagonal matrix. If the fracture were rotationally invariant, then $Z_{12} \equiv 0$ and $Z_{T_1} = Z_{T_2} \equiv Z_T$. The rotation until Z_{12} vanishes is equivalent to rotating the coordinate system in a monoclinic (up-down symmetric) medium about the x_3 -axis until c_{45} vanishes. In such a coordinate system, vertically propagating shear waves polarized in the 1-direction are uncoupled from those polarized in the 2-direction. In addition the ellipse governing propagation of crossplane wave in the 1-, 2-plane has its principle directions in the 1- and 2-directions.

In two dimensions, $\underline{\mathbf{Z}}_T$ and $\underline{\mathbf{Z}}_N$ are 2×2 matrices that depend on tangential slip compliance in the 1, 3 plane, $Z_T > 0$ (with $Z_{12} = 0$), and on the normal slip compliance, $Z_N > 0$, respectively. The linear slip conditions are

$$\begin{aligned} u_1|_{0+} &= u_1|_{0-} + Z_T \sigma_5, \\ \sigma_3|_{0+} &= \sigma_3|_{0-}, \\ \sigma_5|_{0+} &= \sigma_5|_{0-}, \\ u_3|_{0+} &= u_3|_{0-} + Z_N \sigma_3, \end{aligned}$$

which after differentiating by time may be rewritten,

$$\begin{aligned} v_1|_{0-} &= v_1|_{0+} + i\omega Z_T \sigma_5, \\ \sigma_3|_{0-} &= \sigma_3|_{0+}, \\ \sigma_5|_{0-} &= \sigma_5|_{0+}, \\ v_3|_{0-} &= v_3|_{0+} + i\omega Z_N \sigma_3, \end{aligned} \tag{A-10}$$

i.e.,

$$\underline{\mathbf{Z}}_T = \begin{bmatrix} Z_T & 0 \\ 0 & 0 \end{bmatrix}, \quad \underline{\mathbf{Z}}_N = \begin{bmatrix} 0 & 0 \\ 0 & Z_N \end{bmatrix}, \tag{A-11}$$

in equation (A-5). For this case, there is a simple form for the terms $\underline{\mathbf{X}}^{-1} \underline{\mathbf{Z}}_T \underline{\mathbf{Y}}$ and $\underline{\mathbf{Y}}^{-1} \underline{\mathbf{Z}}_N \underline{\mathbf{X}}$ that appear in the solution (A-7) for $\underline{\mathbf{T}}$ and $\underline{\mathbf{R}}$:

$$\begin{aligned} \underline{\mathbf{X}}^{-1} \mathbf{Z}_T \underline{\mathbf{Y}} &= \mathbf{Z}_T \begin{bmatrix} X_{11}^{-1} \\ X_{21}^{-1} \end{bmatrix} [Y_{11} \quad Y_{12}] \\ &= \frac{\mathbf{Z}_T}{|\underline{\mathbf{X}}|} \begin{bmatrix} X_{22} \\ -X_{21} \end{bmatrix} [Y_{11} \quad Y_{12}], \\ \underline{\mathbf{Y}}^{-1} \mathbf{Z}_N \underline{\mathbf{X}} &= \mathbf{Z}_N \begin{bmatrix} Y_{12}^{-1} \\ Y_{22}^{-1} \end{bmatrix} [X_{21} \quad X_{22}] \\ &= \frac{\mathbf{Z}_N}{|\underline{\mathbf{Y}}|} \begin{bmatrix} -Y_{12} \\ Y_{11} \end{bmatrix} [X_{21} \quad X_{22}]. \end{aligned} \tag{A-12}$$

In general, $\underline{\mathbf{X}}$ and $\underline{\mathbf{Y}}$ may be written explicitly in terms of the solutions of Christoffel equations for the vertical slownesses and their associated polarization vectors for a given horizon-

tal slowness (Schoenberg and Protazio, 1992). However, for an isotropic medium with compressional speed α , shear speed β , and density ρ , the explicit expressions reduce to

$$\begin{aligned} \underline{\mathbf{X}} &= \begin{bmatrix} \alpha p_1 & \beta p_{3S} \\ -\rho \alpha (1 - 2\beta^2 p_1^2) & 2\rho \beta^3 p_1 p_{3S} \end{bmatrix}, \\ \underline{\mathbf{Y}} &= \begin{bmatrix} -2\rho \alpha \beta^2 p_1 p_{3P} & -\rho \beta (1 - 2\beta^2 p_1^2) \\ \alpha p_{3P} & -\beta p_1 \end{bmatrix}, \end{aligned} \tag{A-13}$$

$$p_{3S} \equiv \sqrt{\frac{1}{\beta^2} - p_1^2}, \quad p_{3P} \equiv \sqrt{\frac{1}{\alpha^2} - p_1^2},$$

with,

$$|\underline{\mathbf{X}}| = \rho \alpha \beta p_{3S}, \quad |\underline{\mathbf{Y}}| = \rho \alpha \beta p_{3P}.$$

APPENDIX B

EXPLICIT MODELING OF SLIP BOUNDARY CONDITIONS

To verify the effective medium model of a fault we need to be able to compare the results it produces with synthetics generated using an explicit application of the boundary condition. The latter is difficult to implement for arbitrary fault orientation (hence the need for the effective medium theory). However, for the particular case of the fault plane lying parallel to one of the finite-difference grid axes, explicit boundary conditions are relatively straightforward to implement. In this Appendix we outline how this is done.

Figure B.1 shows the fault passing through one cell in two dimensions. Differentiating the linear slip model with respect to time gives,

$$\begin{aligned} \Delta v_x &= \mathbf{Z}_T \frac{\partial \sigma_{xz}}{\partial t}, \\ \Delta v_z &= \mathbf{Z}_N \frac{\partial \sigma_{zz}}{\partial t}, \end{aligned} \tag{B-1}$$

where $\Delta v_x = \partial \Delta u_x / \partial t$ is the horizontal slip velocity and Δv_z is the vertical slip velocity. Thus, for a fault invariant in the x -direction, we obtained the discrete equations

$$\begin{aligned} \frac{\Delta v_x}{\Delta x} &= s_{11} \frac{\Delta \sigma_{xx}}{\Delta t} + s_{13} \frac{\Delta \sigma_{zz}}{\Delta t}, \\ \frac{\Delta v_z}{\Delta z} &= s_{13} \frac{\Delta \sigma_{xx}}{\Delta t} + \left(s_{13} + \frac{\mathbf{Z}_N}{\Delta z} \right) \frac{\Delta \sigma_{zz}}{\Delta t}, \\ \frac{\Delta v_x}{\Delta z} + \frac{\Delta v_z}{\Delta x} &= \left(s_{55} + \frac{\mathbf{Z}_T}{\Delta z} \right) \frac{\Delta \sigma_{zz}}{\Delta t}, \end{aligned} \tag{B-2}$$

where s_{IJ} is the compliance matrix of the background medium. Rewriting these equations using stiffnesses and second-order differences yields the following expressions for the cell containing the fault plane

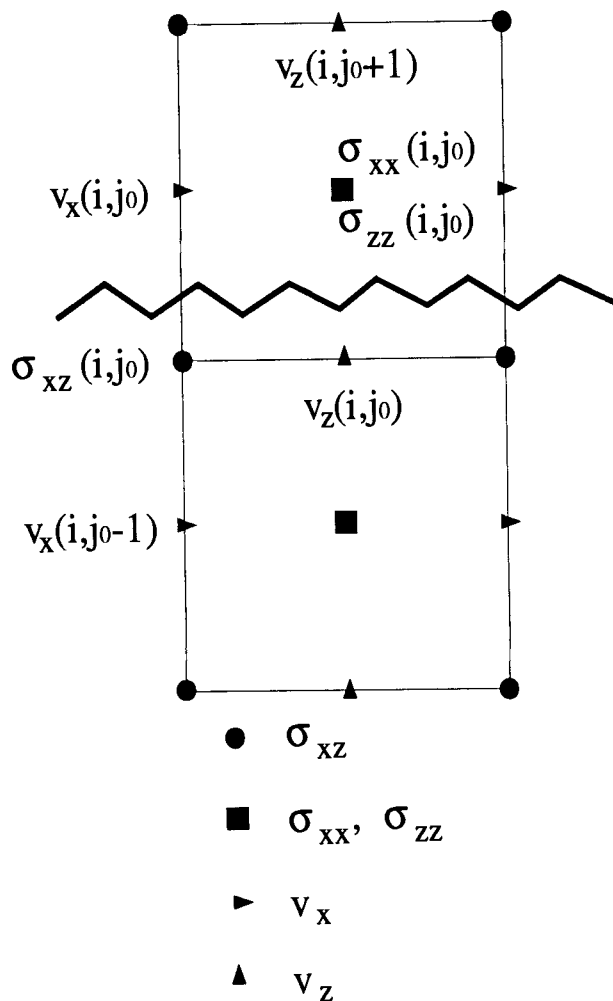


FIG. B.1. The fault (jagged line) passing horizontally through a cell of the finite-difference grid. To the accuracy of the finite-difference grid, the vertical location of the fault plane is taken as being between $v_z(i, j)$ and $v_x(i, j)$. The slip occurs between the labeled vertical and horizontal velocity nodes.

$$\begin{aligned}
\frac{\Delta\sigma_{xx}}{\Delta t}(i, j_0) &= \left(c_{11}(i, j_0) - \frac{c_{13}^2(i, j_0)Z_N/\Delta z}{(1 + c_{33}(i, j_0)Z_N/\Delta z)} \right) && + \left(\frac{c_{33}(i, j_0)}{1 + c_{33}(i, j_0)Z_N/\Delta z} \right) && \text{(B-3)} \\
&\times \left(\frac{v_x(i+1, j_0) - v_x(i, j_0)}{\Delta x} \right) && \times \left(\frac{v_z(i, j_0+1) - v_z(i, j_0)}{\Delta z} \right), \\
&+ \left(\frac{c_{13}(i, j_0)}{1 + c_{33}(i, j_0)Z_N/\Delta z} \right) \\
&\times \left(\frac{v_z(i, j_0+1) - v_z(i, j_0)}{\Delta z} \right), \\
\frac{\Delta\sigma_{zz}}{\delta t}(i, j_0) &= \left(\frac{c_{13}(i, j_0)}{(1 + c_{33}(i, j_0)Z_N/\Delta z)} \right) \\
&\times \left(\frac{v_x(i+1, j_0) - v_x(i, j_0)}{\Delta x} \right)
\end{aligned}$$

$$\begin{aligned}
\frac{\Delta\sigma_{xz}}{\delta t}(i, j_0) &= \left(\frac{c_{13}(i, j_0)}{(1 + c_{13}(i, j_0)Z_T/\Delta z)} \right) \\
&\left(\frac{v_x(i, j_0) - v_x(i, j_0-1)}{\Delta z} + \frac{v_z(i, j_0) - v_z(i-1, j_0)}{\Delta x} \right).
\end{aligned}$$

For a horizontal fault, these equations hold for all $0 \leq i \leq i_{\max}$. However, for $j \neq j_0$ we use the usual constitutive equations [which may be obtained from equation (B-3) by setting $Z_N = Z_T = 0$].